THESEUS1 modulates cell wall stiffness and abscisic acid production in *Arabidopsis thaliana*

Laura Bacete[a] (ORCID), Julia Schulz[a] (ORCID), Timo Engelsdorf[b] (ORCID), Zdenka Bartosova[a], Lauri Vaahtera[a], Guqi Yan[c,1] (ORCID), Joachim Matthias Gerhold[d], Tereza Tichá[a], Camilla Øvstebø[a], Nora Gigli-Bisceglia[a,2], Svanhild Johannessen-Starheim[a], Jeremie Margueritat[c], Hannes Kollist[d], Thomas Dehoux[c] (ORCID), Scott A. M. McAdam[e], and Thorsten Hamann[a,3] (ORCID)

[a]Institute for Biology, Faculty of Natural Sciences, Norwegian University of Science and Technology, 7491 Trondheim, Norway; [b]Division of Plant Physiology, Department of Biology, Philipps University of Marburg, 35043 Marburg, Germany; [c]Institut Lumière Matière, UMR5306, Université Lyon, 1-CNRS 69622 Villeurbanne, France; [d]Institute of Technology, University of Tartu, 50411 Tartu, Estonia; and [e]Department of Botany and Plant Pathology, Purdue University, West Lafayette, IN 47907

Plant cells can be distinguished from animal cells by their cell walls and high-turgor pressure. Although changes in turgor and the stiffness of cell walls seem coordinated, we know little about the mechanism responsible for coordination. Evidence has accumulated that plants, like yeast, have a dedicated cell wall integrity maintenance mechanism. It monitors the functional integrity of the wall and maintains integrity through adaptive responses induced by cell wall damage arising during growth, development, and interactions with the environment. These adaptive responses include osmosensitive induction of phytohormone production, defense responses, as well as changes in cell wall composition and structure. Here, we investigate how the cell wall integrity maintenance mechanism coordinates changes in cell wall stiffness and turgor in *Arabidopsis thaliana*. We show that the production of abscisic acid (ABA), the phytohormone-modulating turgor pressure, and responses to drought depend on the presence of a functional cell wall. We find that the cell wall integrity sensor THESEUS1 modulates mechanical properties of walls, turgor loss point, ABA biosynthesis, and ABA-controlled processes. We identify RECEPTOR-LIKE PROTEIN 12 as a component of cell wall integrity maintenance–controlling, cell wall damage–induced jasmonic acid (JA) production. We propose that THE1 is responsible for coordinating changes in turgor pressure and cell wall stiffness.

plant cell wall | cell wall integrity | abscisic acid | THE1

Plant cell walls are chemically complex structures, changing their composition and structure in a highly dynamic, adaptive manner to meet different biological functions (1). The walls provide structural support during development, are frequently the first line of defense in response to environmental stress, and constrain the high-turgor pressure in cells, pressures that commonly exceed the levels found in bicycle tires (2–4). Relative abundance and organization of wall components determines the mechanical characteristics of cell walls and varies between plant species, cell types, and developmental stages. Major components include cellulose microfibrils (the main load-bearing elements), hemicelluloses, pectins, lignin, and cell wall proteins (5). While the mechanical characteristics of epidermal cell walls are well-described, knowledge regarding the mechanical properties of cell walls in subepidermal tissues in vivo is limited (3). Recently, Brillouin microscopy, which is well-established in materials sciences, has been adapted for use in life sciences to address this lack of knowledge (6, 7). This label-free, quantitative microscopy technology takes advantage of the Brillouin light scattering (BLS) effect. It is based on characterizing the interactions of a laser light with the sample, which involve picosecond–timescale density fluctuations due to spontaneous molecular motions. Since the interactions couple photons to longitudinal phonons in the sample, variations in the scattering spectra of the laser light can be interpreted as a response of the sample to an infinitesimal, uniaxial compression. This response can be integrated with the refractive index to extract the Brillouin elastic contrast ($\bar{\nu}_B$), which can reveal changes in stiffness of the sample examined. Variations in refractive index and mass density in tissues are usually small, leading to negligible changes in Brillouin shifts (8). For this reason, we interpret changes in the Brillouin shifts as the signature of drastic changes in cell wall stiffness.

Knowledge regarding the mechanisms regulating plant cell wall composition and structure has increased recently. However, our understanding of how changes in composition and structure result in modifications to the mechanical characteristics of the cell wall, such as stiffness, is still limited (3). More importantly, we know even less about the mechanisms responsible for controlled changes in cell wall stiffness. The plant cell wall integrity (CWI) maintenance mechanism is of interest in this context because it could contribute to controlling cell wall stiffness in plants. The mechanism monitors the functional integrity of cell walls during growth, development, and interactions of plants with

> **Significance**
>
> Plants need to constantly adapt to a changing environment. Adaptation includes responses to biotic and abiotic stress. Key elements determining the response to abiotic stress are the cell walls surrounding all plant cells and the phytohormone abscisic acid, which influence turgor pressure in plants. Turgor pressure in plant cells is much higher than in animal cells and a key driver of plant growth and development. Here, we investigate the mechanism regulating cell wall stiffness and coordinating changes in stiffness and turgor with abscisic acid production. We characterize key elements of the mechanism and dissect its mode of action. This knowledge will enable us to improve plant resistance to drought stress, which is necessary due to our changing environment.

PLANT BIOLOGY

their environment (9). Upon the impairment of integrity, the mechanism initiates adaptive changes in cell wall composition and structure as well as cellular metabolism, including the induction of jasmonic acid (JA) and salicylic acid (SA) production. Importantly, all these responses can be suppressed by performing cotreatment with osmotica, which reduces turgor pressure and is similar to observations made in *Saccharomyces cerevisiae* (10–15). JA has also been implicated in regulating responses to mechanostimulation, in addition to its more established role in biotic stress responses, illustrating the relevance of mechanoperception for biotic stress responses (16). Different components involved in mechano- and turgor sensing are required for CWI maintenance in *Arabidopsis thaliana* (13). Among them are members of the *Catharanthus roseus* receptor-like, kinase 1–like (*Cr*RLK1L) family, which contribute to CWI maintenance in different biological processes (17). Two family members, FERONIA (FER) and THESEUS1 (THE1), are of particular interest. THE1 is required for hypocotyl cell elongation, responses to cell wall damage (CWD) induced by inhibition of cellulose biosynthesis, and during plant–pathogen interactions (13, 18, 19). THE1 interacts with the peptide ligand RAPID ALAKALINIZATION FACTOR 34 to also control lateral root initiation and is dependent on FER activity (20). FER integrates and coordinates a large number of cellular processes during development and response to stress. The processes include CWI maintenance, coordination of changes in cell wall composition with vacuolar expansion, and modulation of abscisic acid (ABA) production, a phytohormone required for adaptation to drought stress (21–24). FER delivers these highly specific, context-dependent functions by acting as a scaffold protein interacting with a large number of signaling peptides and coreceptors, often in a pH-dependent manner (25).

ABA is essential for plant adaptation to drought stress and has therefore been investigated extensively in guard cells (26). ABA biosynthesis, which primarily occurs in mesophyll cells, is well-characterized and requires enzymes like ABA DEFICIENT 2 (ABA2) (27, 28). Newly produced ABA binds to the ligand-binding poket of the receptors known as PYRABACTIN RESISTANCE 1 (PYR1)/PYRABACTIN RESISTANCE 1-LIKE (PYL) /REGULATORY COMPONENT OF ABA RECEPTOR (RCAR). The binding induces a structural modification which allows the interaction of the ligand-receptor complex with a member of the subgroup A of type 2C protein phosphatases (PP2Cs), leading to the inhibition of its phosphatase activity. PP2C inhibition allows the autophosphorylation and consequent activation of SNF1-RELATED PROTEIN KINASES 2 (SnRK2s) such as OPEN STOMATA1, which in turn activates the SLOW ANION CHANNEL1 through phosphorylation. This consecutively induces the release of anions (Cl^- and NO_3^-) causing membrane depolarization. Depolarization causes release of K^+ ions through K^+ channels, resulting in water leaving the guard cell and turgor pressure being reduced (29). This simplified overview highlights the extensive knowledge available about ABA biosynthesis and signaling. However, understanding of the osmosensitive processes responsible for induction of ABA production in response to drought is very limited (28, 30).

We hypothesized previously that interactions between *Cr*RLK1Ls and ABA-mediated processes may coordinate adaptive changes in turgor pressure and cell wall stiffness in response to cell expansion or shrinking (9). Here, we investigated changes in cell wall stiffness in vivo in subepidermal tissues in *Arabidopsis* seedling roots, established the function of THE1 in the regulation of stiffness, and proceeded to show that THE1 also modulates ABA production induced by interactions between the plasma membrane and the cell wall. Using a transcriptomics-based approach, we identified *RECEPTOR-LIKE PROTEIN 12* (*RLP12*) as a component of the CWI maintenance mechanism and characterized RLP12 function in cell wall metabolism, response to CWD, and ABA-mediated processes.

Results

THE1 Modulates Cell Wall Stiffness in *Arabidopsis* Seedling Roots.

To investigate the interplay between cell wall stiffness and turgor pressure in vivo, we treated *A. thaliana* seedlings with the cellulose biosynthesis inhibitor isoxaben (ISX) to cause CWD in a tightly controlled manner and impair CWI, sorbitol to reduce turgor pressure, or a combination of both and studied the effects using Brillouin microscopy (*SI Appendix*, Fig. S1) (13, 31). Wild-type (Columbia-0 [Col-0]) seedlings were treated with ISX for 6 h in a pilot study. Longitudinal scans with a Brillouin microscope along the treated seedling roots at three different depths detected the highest BLS contrast in the stele 450 μm from the root tip (*SI Appendix*, Fig. S2 *A* and *B*). Subsequently, seedling roots were mock, ISX, sorbitol, or ISX/sorbitol treated for 6 h, and radial scans were performed in this area. Light microscopy–based studies revealed that the different treatments have pronounced effects on seedling root morphology in this area (*SI Appendix*, Fig. S2C). Mock- and sorbitol-treated roots appeared normal, while ISX-treated roots appeared swollen and sorbitol/ISX-treated ones exhibited reduced swelling. Radial scans with a Brillouin microscope revealed in roots treated with ISX- or sorbitol-pronounced reductions in stiffness in the stele in this area (Fig. 1 *A* and *B*). By contrast, stiffness in Col-0 roots cotreated with ISX and sorbitol was similar to mock-treated controls. In *isoxaben resistant1-1* (*ixr1-1*) mock-, ISX-, and sorbitol-treated roots, stiffness levels differed from wild type, but responses to treatments were qualitatively equivalent to those observed in Col-0. The observed changes in stiffness might be modulated by dynamic interactions between the plasma membrane and the cell wall. We hypothesized that THE1 could contribute to these interactions, since it is membrane localized and required for responses to ISX (13, 18). Mock-treated *theseus1-1* (*the1-1*) (loss-of-function allele) roots exhibited pronouncedly lower stiffness compared to wild type, and treatments induced no significant changes compared to mock-treated roots. ISX and sorbitol treatments of *the1-4* (gain-of-function allele) roots resulted in pronounced differences compared to mock controls and were similar to the effects observed in Col-0 roots (32). Importantly, combined ISX/sorbitol treatments resulted in stiffness levels similar to those observed in sorbitol-only–treated roots. ISX (cell wall weakening) and sorbitol (turgor reduction) treatments of Col-0 led to similarly reduced cell wall stiffness in subepidermal tissue layers, while combined treatments led to enhanced stiffness. These observations suggest that changes in turgor pressure and ISX treatment affect stiffness through separate processes and that these processes may jointly modulate stiffness in subepidermal tissue layers. THE1 seems to be required for regulating stiffness during growth and following CWD induced by ISX, based on the phenotypes observed in *the1-1* seedling roots. While loss of THE1 has no effect on stiffness changes induced by ISX/sorbitol cotreatment, overactive THE1 prevents these stiffness increases. This suggests that THE1 indirectly influences the process controlling the response to ISX/sorbitol cotreatments, possibly as a consequence of THE1 function in modulating responses to ISX.

THE1 Is a Negative Regulator of ABA Biosynthesis in Seedlings.

Hyperosmotic stress induces ABA biosynthesis and reduced turgor pressure, while ISX treatment triggers JA production in a THE1-dependent manner (10, 11, 33–35). We treated seedling roots as before and used promoter reporter constructs to determine, if JA, ABA response levels and *THE1* expression change in the root area where stiffness changes were observed (20, 36, 37). Expression of the promoter p*THE1::YFP* reporter was detectable in mock-treated seedling root tips and induced by ISX treatment in the region where changes in stiffness had
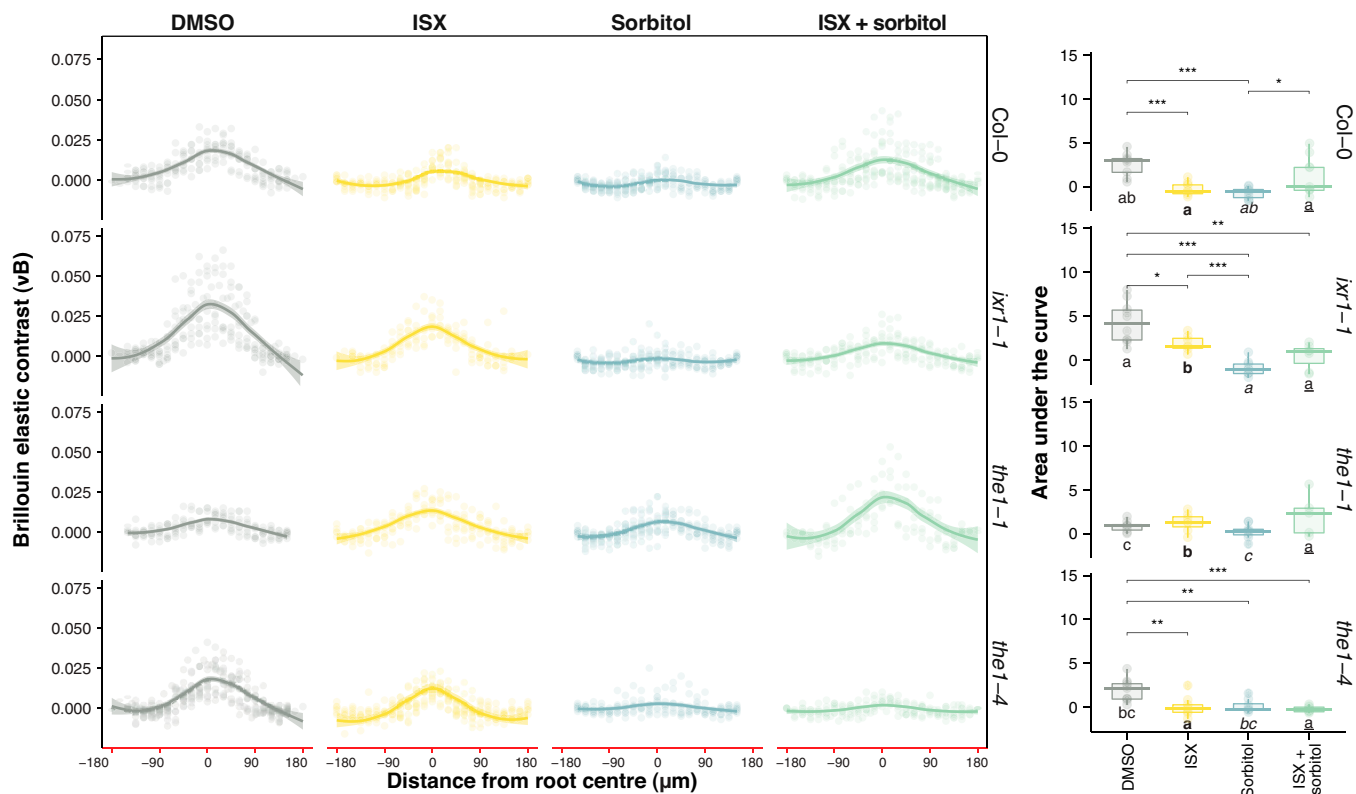
Fig. 1. Changes in stiffness of *A. thaliana* root cell walls are mediated by THE1. Brillouin elastic contrasts measurements ($\bar{v}_B$) across the radial axis in the basal meristem–transition zone of *A. thaliana* seedling roots from Col-0, *ixr1-1*, *the1-1*, and *the1-4*. Brillouin measurements were performed after 6 h of treatment, as indicated. Dots represent individual measurements ($n > 10$), with lines representing corresponding regression curves (LOESS adjustment) with a 95% CI (shadowed). Areas under the curves were calculated for each root ($n > 10$). Asterisks indicate significance levels, allowing the comparison of treatment effects within the same genotype (Kruskal–Wallis test with Dunn post hoc analysis, *$P < 0.05$, **$P < 0.01$, and ***$P < 0.001$), whereas letters indicate statistically significant different groups ($P < 0.05$) for the same treatment between different genotypes (i.e., by columns).

been detected (Fig. 2*A*). p*THE1::YFP* expression was particularly pronounced after ISX treatment in the stele and less in the surrounding tissue layers. Sorbitol cotreatment seemed to reduce ISX-induced expression to a level observed in the sorbitol-treated roots. The JA reporter (p*JASMONATE-ZIM-DOMAIN PROTEIN 10* [p*JAZ10*]::*YFP*) exhibited ISX-induced, sorbitol-sensitive expression in and around the stele of seedling roots in a similar region like p*THE1*::YFP (Fig. 2*B*). The ABA reporter p*RAB GTPASE HOMOLOG 18–1* (p*RAB18*)::*GUS-GFP* was preferentially expressed in subepidermal cell layers in ISX-, sorbitol- and ISX/sorbitol-treated seedling roots (Fig. 2*C*).

We proceeded to investigate if THE1 modulates sorbitol- and ISX-induced ABA and JA biosynthesis by performing time course experiments and measuring both phytohormones simultaneously in Col-0, *the1-1*, and *the1-4* seedlings (Fig. 2*D*). In mock-, sorbitol-, and ISX/sorbitol-treated seedlings JA production was not increased. In ISX-treated *the1-1* seedlings, JA production was reduced compared to Col-0 controls, while it was enhanced in *the1-4*. ABA production was not increased in mock- or ISX-treated seedlings. In sorbitol and ISX/sorbitol-treated Col-0 and *the1-4* seedlings, ABA production was transiently increased in a similar manner. However, in *the1-1* seedlings, the increases were enhanced in a pronounced manner. These results suggested that THE1 acts as a positive regulator of JA production in response to CWD and negative regulator of ABA production induced by hyperosmotic stress.

JA- and ABA-based processes interact to mediate plant adaptation to drought (38). Therefore, we investigated if ISX- or sorbitol-induced JA and ABA production modulate each

other and characterized the function of THE1 in this context. To achieve these aims, JA and ABA production were quantified in *the1-1*, *the1-4*, *aba2*, *enhanced response to aba 1* (*era1*), or *allene oxide synthase* (*aos*, deficient in JA production) seedlings mock, ISX, sorbitol, or ISX/sorbitol treated for 6 h (Fig. 2*E*). In mock-treated seedlings, no pronounced changes in JA and ABA production were detected. The effects of manipulating THE1 activity on JA and ABA production were comparable to the results presented in Fig. 2*D*. In ISX-treated *aos* seedlings, JA production was not detectable. While ISX-treated *aba2* and *era1* seedlings exhibited slightly enhanced JA production compared to Col-0, the effects were less pronounced than in *the1-4* seedlings. ABA was not detectable in sorbitol- and ISX/sorbitol-treated *aba2* seedlings. Changes in ABA production were limited in *aos* and *era1-2* after sorbitol or ISX/sorbitol treatments. These results indicate that genetically manipulating ABA and JA biosynthesis affects induction of the corresponding phytohormone by sorbitol or ISX. However, the effects are less pronounced than those observed when manipulating THE1 activity, suggesting that the effects observed are not direct. Particularly, for *aba2-1*, the observed effects are probably indirect because of effects of the mutation on plant growth, which in turn affect response to ISX. Interactions between JA- and ABA-mediated processes responsible for adaptation to drought stress have been described before and could be responsible for the effects we observe here (38).

We followed up further by investigating how manipulation of CWI signaling and ABA biosynthesis affects downstream transcriptional responses induced by ISX or sorbitol. Expression levels of *RAB18* and the ISX-induced *TOUCH4* (*TCH4*) gene
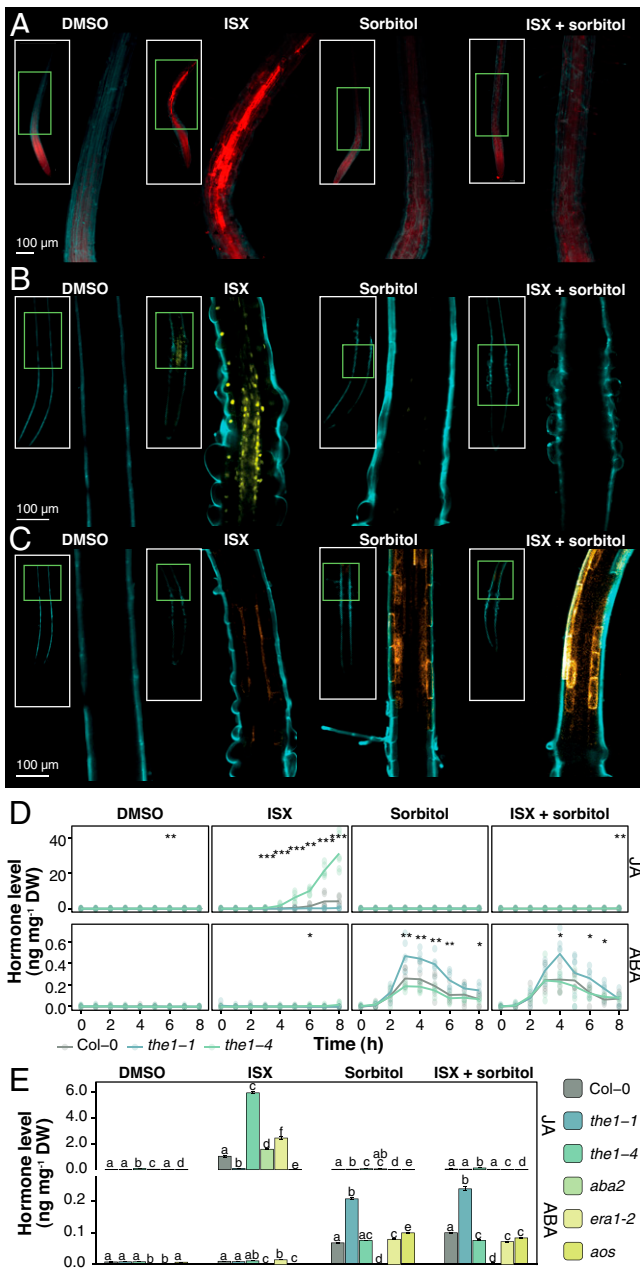
Bacete et al.
THESEUS1 modulates cell wall stiffness and abscisic acid production
in *Arabidopsis thaliana*

PNAS | 3 of 10
https://doi.org/10.1073/pnas.2119258119

PLANT BIOLOGY

Fig. 2. Hyperosmotic and CWI signaling modulate JA/ABA induction and reporter gene expression. (*A–C*) Confocal light microscope images of seedlings expressing *pTHE1::YFP* (red) (*A*), *pJAZ10::YFP* (JA reporter, yellow) (*B*), or *pRAB18::GFP-GUS* (ABA reporter, orange) (*C*) exposed to different treatments, as indicated in the figure. Root cell walls were counter stained with Calcofluor White Solution (cyan). (*D*) Quantification of ABA and JA levels in nanogram hormone per milligram dry weight (DW). Genotypes and treatments are indicated in the figure. Points represent individual measurements, and lines show average values (n = 3). Asterisks indicate statistically significant differences (*$P < 0.05$, **$P < 0.01$, and ***$P < 0.001$; Kruskal–Wallis test). (*E*) Phytohormone levels in whole seedlings with treatments (6 h) and genotypes indicated in the figure; Average values (n = 4) ± SEM. Letters indicate significant, within-group differences between genotypes (Kruskal–Wallis test with Dunn post hoc analysis, $P < 0.05$).

were used as readouts (39). We characterized the expression of *RAB18* and *TCH4* in *the1-1*, *the1-4*, and ABA-related (*aba2* and *era1*) mutant seedlings mock, ISX, or sorbitol treated for 6 h (*SI Appendix,* Fig. S3). *RAB18* expression did not change in a pronounced way in mock-treated seedlings and was not detectable in *aba2*, while a limited expression increase was detectable

in ISX-treated *era1-2* seedlings. *RAB18* expression was elevated in sorbitol-treated *the1-1* seedlings but similar to Col-0 in ISX/sorbitol-treated *the1-1* seedlings. In *the1-4* seedlings, *RAB18* expression was reduced in response to both treatments compared to Col-0 seedlings. *RAB18* expression was not detectable in sorbitol-treated *aba2* seedlings. In sorbitol-treated *era1-2* seedlings, expression was similar to Col-0 and reduced in response to ISX/sorbitol treatment. The transcriptional effects observed for *TCH4* were pronouncedly different. In mock-treated seedlings, *TCH4* expression was elevated only in *the1-1* seedlings. In sorbitol and ISX/sorbitol-treated seedlings, all genotypes examined exhibited reduced *TCH4* expression compared to Col-0 seedlings. Expression of *TCH4* was reduced similarly in *the1-1* and *the1-4* seedlings upon ISX treatment, while it was enhanced both in *aba2* and *era1-2* seedlings. The results indicate that ABA production (*aba2*) is required for *RAB18* expression, while ERA1 activity seems not essential. Manipulating THE1 activity has similar effects on *RAB18* expression, like on ABA production, reinforcing the notion that THE1 is a negative regulator of ABA-mediated processes. These results imply that ABA2 and ERA1 act as negative regulators of *TCH4* expression, while THE1 has apparently no direct regulatory role.

RLP12 Regulates CWD-Induced JA Production. We performed an RNA sequencing experiment to identify additional genes required for CWI maintenance. After growing seedlings for 6 d in liquid culture, they were mock-, ISX-, sorbitol- or ISX/sorbitol treated for 1 h. We then proceeded to identify genes whose expression changes in response to ISX or sorbitol treatments but does not significantly change in cotreated seedlings (Fig. 3*A*). Expression patterns of 10 genes meet these criteria with two of them (*PROPEPTIDE1* and *2*) previously implicated in CWI maintenance (13). This group also included *RLP12*, which belongs to a gene family with 57 members and has been implicated in biotic and osmotic stress responses (40). Time course experiments with mock-, ISX-, sorbitol-, and ISX/sorbitol-treated Col-0 and *ixr1-1* seedlings were performed to validate transcriptomics-derived expression data for *RLP12* using qRT-PCR. ISX induced *RLP12* expression in a sorbitol-sensitive manner in Col-0 but not in *ixr1-1* seedlings (Fig. 3*B*). A *pRLP12::GUS-GFP* reporter construct was generated, and seedlings expressing the construct were treated in the same manner for 6 h (Fig. 3*C*). Analysis of reporter construct expression suggested that *RLP12* expression is induced by ISX in a sorbitol-sensitive manner in the stele of the root transition/elongation zone (similar to p*THE1::YFP*) and an area in the differentiated seedling root (Fig. 3*D*). We used three different homozygous transfer DNA (T-DNA) insertion mutants which are knock-outs for *RLP12* gene (*SI Appendix,* Fig. S4*A*), and determined ABA and JA production in seedlings after mock, ISX, sorbitol, or ISX/sorbitol treatments (*SI Appendix*, Fig. S4*B*). Reduced JA production was detected after ISX treatment, while ABA production did not exhibit pronounced differences compared to Col-0 controls. In addition, time course experiments were performed to investigate how loss of *RLP12* affects temporal dynamics of phytohormone induction by the different treatments (Fig. 3*D*). JA production was less induced by ISX in *rlp12-1* seedlings than in Col-0, while ABA production did not differ in a pronounced manner. These results indicate that *RLP12* is required for ISX-induced JA production; is expressed in the same region of the root in an ISX-induced, sorbitol-sensitive manner like THE1; and implicate RLP12 in CWI maintenance.

Cell Wall Integrity and ABA Homeostasis Modulate Turgor Loss Points and Cell Wall Metabolism in Adult Plants. The available data implicate RLP12 and THE1 in osmosensitive CWI maintenance and, possibly, ABA-mediated processes in seedlings. To clarify their respective roles in more detail, we initiated a
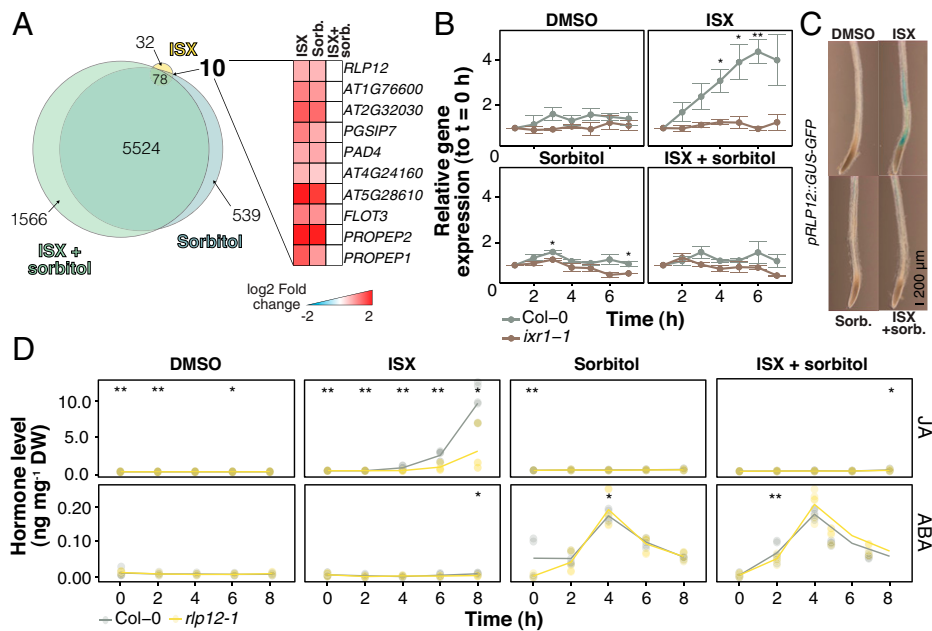
Bacete et al.
THESEUS1 modulates cell wall stiffness and abscisic acid production
in *Arabidopsis thaliana*

Fig. 3. RLP12 regulates JA production induced by CWD. (*A*) Results of RNA sequencing–based gene expression analysis of seedlings treated as indicated in the figure. (*B*) Changes in expression levels of *RLP12* over time in seedlings treated, as highlighted in the figure. Average values ± SEM of four independent experiments with three technical replicates (*n* = 12) are shown. Asterisks indicate statistically significant differences (*$P < 0.05$ and **$P < 0.01$; ANOVA with Tukey correction for multiple comparisons). (*C*) *Arabidopsis* seedling roots transformed with *pRLP12::GFP-GUS* and treated as indicated in the figure. (*D*) Quantification of JA and ABA levels in nanogram hormone per milligram dry weight (DW) in wild-type and *rlp12-1* seedlings. Points represent individual measurements, and lines show average values (*n* = 3). Asterisks indicate statistically significant differences (*$P < 0.05$ and **$P < 0.01$; Kruskal–Wallis test).

phenotypic characterization of RLP12 and THE1 in seedlings and adult plants. *aba2* and *ABA receptor mutant pyr1pyl1ply2-pyl4pyl5pyl8* (*pyr pyl*)-derived plant materials were included as controls where appropriate, since they affect ABA biosynthesis and signaling (41, 42). The roles of RLP12 and THE1 in seedling root growth and ABA perception were assessed by transferring 6-d-old Col-0, *pyr pyl*, *the1-1*, *the1-4*, and *rlp12-1* seedlings onto plates with or without ABA (*SI Appendix*, Fig. S5A). Seedlings from all genotypes examined exhibited root growth rates similar to Col-0. While *pyr pyl* seedling root growth was resistant to ABA, Col-0 root growth was inhibited. Root growth inhibition by ABA was more pronounced in *rlp12-1* than in Col-0. However, *the1-1* and *1-4* root growth seemed even more sensitive to ABA than *rlp12-1*. These results indicate that THE1 and RLP12 are not essential for root growth, and both THE1 and RLP12 seem to act as negative regulators of ABA-mediated root growth inhibition. Changes in conductance induced by ABA were characterized in Col-0, *the1-1*, *the1-4*, and *rlp12-1* stomata, while induction by light was also investigated in *aba2* (Fig. 4 *A* and *B*). While pronounced differences to Col-0 were detected for *aba2* in response to light induction, none were detectable for *the1* and *rlp12-1*. However, *the1-1* and *the1-4* stomata did exhibit responses qualitatively opposite to each other upon exposure to both light and ABA. Turgor loss point has been suggested as a useful tool to assess drought stress resistance and turgor levels in plants (43). We determined turgor loss points in leaves of Col-0, *aba2*, *the1-1*, *the1-4*, and *rlp12-1* adult plants (Fig. 4*C*) and found that only *the1-1* leaves exhibited a pronounced increase, implying enhanced susceptibility to drought stress. Cell wall monosaccharides and cellulose were quantified in Col-0, *aba2*, *the1-1*, *the1-4*, and *rlp12-1* leaves and seedlings to determine if these genes have essential roles in the regulation of cell wall composition (Fig. 4*D* and *SI Appendix*, Fig. S5C). No pronounced changes were detected in *the1-1*, *the-4*, or *rlp12-1* seedlings or leaves. In *aba2* leaves, monosaccharide composition was similar to Col-0, but cellulose amounts were

reduced. A similar reduction in cellulose has been reported for *aba1* plants (44). These results suggest that THE1 and RLP12 are required for ABA-mediated processes during seedling root growth, while they are not essential in adult plants.

Based on the results presented, interactions between cell wall and plasma membrane could be responsible for the induction of ABA production in plants in general. To test this hypothesis, *Arabidopsis* and *Pisum sativum* leaves, mesophyll cells, and protoplasts were mock- or polyethylene glycol (PEG)–treated and ABA production subsequently quantified (Fig. 4*E*). In mock-treated leaves, mesophyll cells and protoplasts ABA production was not enhanced. PEG treatment induced ABA production in leaves and mesophyll cells from both species. However, in protoplasts from both plant species, no increased ABA production was detectable. These results indicate that an intact cell wall is required for the induction of ABA production in mesophyll cells from both *Arabidopsis* and *P. sativum*. Results from early experiments dating back to the 70s and 80s of the last century provide indirect evidence supporting our conclusion (44–46).

Discussion

Here, we have investigated the effects of CWD and turgor manipulation on stiffness in *Arabidopsis* seedling roots, determined the roles of THE1 in the regulation of stiffness, ABA production and ABA-mediated processes, identified RLP12 as a new CWI maintenance component, and established that an intact cell wall is required for hyperosmotic, stress-induced ABA production in plants. The results from the protoplast experiments are exciting because they provide key information enabling us to investigate the mechanism responsible for induction of ABA production, a process regulating plant adaptation to drought (22).

The model shown in Fig. 4*F* uses the knowledge generated here to outline a mechanism capable of coordinating changes in turgor pressure and cell wall stiffness in *Arabidopsis*. Cell wall composition, structure, stiffness, and CWD are interconnected
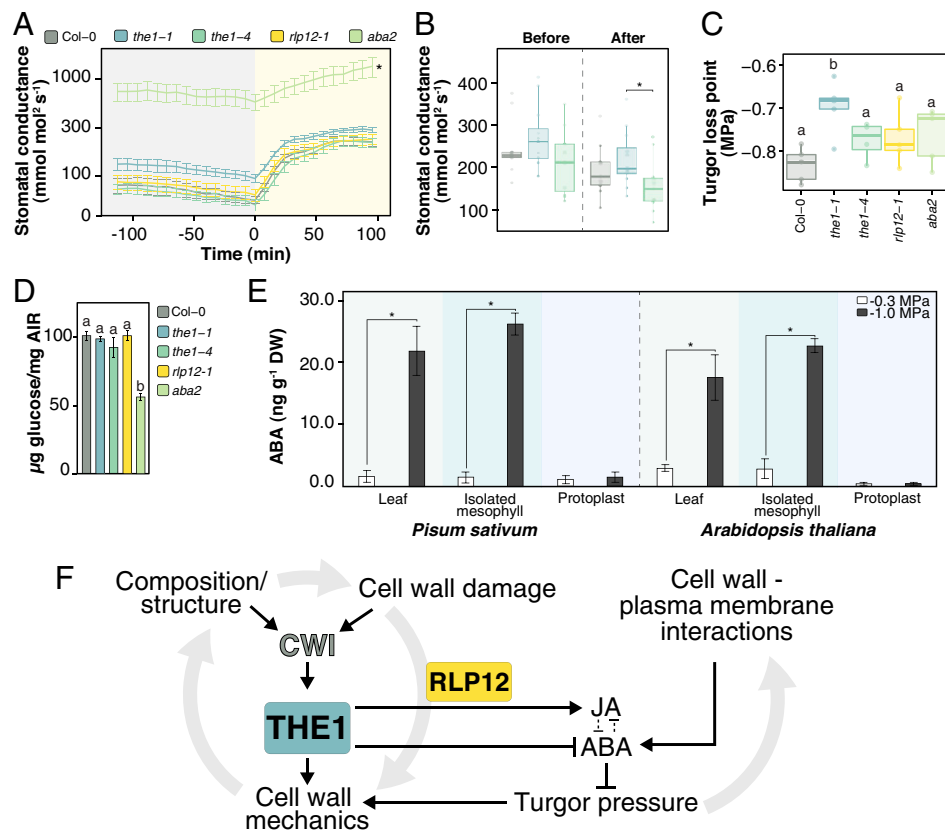
Bacete et al.
THESEUS1 modulates cell wall stiffness and abscisic acid production in *Arabidopsis thaliana*

PNAS | 5 of 10
https://doi.org/10.1073/pnas.2119258119

Fig. 4. CWI and ABA homeostasis modulate turgor loss points and cell wall metabolism in adult plants. (*A* and *B*) Changes in stomatal conductance (dark to light) (*A*) and in response to ABA treatment (*B*); genotypes examined are indicated by color coding in the figure (*n* = 5). Asterisks indicate statistically significant differences (*P < 0.05, ANOVA test with Tukey correction for multiple comparisons). (*C*) Turgor pressure loss point measurements (*n* = 5). Asterisks indicate statistically significant differences (*P < 0.05; ANOVA test with Tukey correction for multiple comparisons). (*D*) Cellulose content of cell walls in leaves; genotypes are indicated in the figure and expressed in micrograms of glucose per milligram of alcohol insoluble fraction (AIR). (*E*) ABA levels in mock- (−0.3 MPa) or osmoticum-treated (−1.0 MPa) *P. sativum* and *A. thaliana* leaves, isolated mesophyll cells, and protoplasts. Average values (*n* = 5) ± SEM. Asterisks indicate statistically significant differences (*P < 0.05, Student's *t* test). (*F*) Simplified model summarizing the roles of THE1 and RLP12 in CWI maintenance, regulation of ABA and JA biosynthesis, as well as modulation of turgor pressure.

and influence CWI. With the objective lens we used, we obtain scattering volumes for the virtually imaged phase array (VIPA) and tandem Fabry–Perot (TFP) setups (*SI Appendix*, Fig. S1) that are too large to discern individual cell walls. However, we observed clear alterations in the mechanical characteristics of the root, which are mostly determined by the cell walls. Interestingly, we did not observe alterations in the *ixr1-1* mutant after ISX treatment, supporting the notion that the alterations are induced by reductions in cellulose production. We conclude, therefore, that stiffness in the stele of seedling roots is reduced in vivo in response to CWD (cellulose biosynthesis inhibition) and reduced turgor pressure (sorbitol). THE1 regulates stiffness changes during seedling root growth and in response to ISX, while affecting those induced by ISX/sorbitol cotreatments. We did not detect global changes in wall monosaccharide composition in *the1* seedlings, suggesting that the effects on stiffness may be caused either by changes in cell wall structure or compositional changes were not detectable with the analytical methods used here. THE1 acts as a positive regulator of JA in response to CWD and a negative one of ABA upon hyperosmotic stress. In *the1-1* leaves, turgor loss point was reduced, suggestive of reduced turgor, which could be explained by increased ABA biosynthesis-reducing turgor pressure, similar to what has been observed in guard cells (26). This implies that THE1 either modulates turgor pressure indirectly by modifying ABA production or THE1 could act as negative regulator of ABA production in adult plants in response to hyperosmotic (drought)

stress. The results from the experiments with *Arabidopsis* and *P. sativum* indicate that interactions between an intact cell wall and the plasma membrane are essential for ABA production. We propose these interactions constitute an on–off switch for activation of ABA biosynthesis. Conversely, the state of the plasma membrane–cell wall continuum would finetune phytohormone biosynthesis via THE1. CWD (or hypoosmotic stress) would cause expansion and induce JA production via THE1, making THE1 a positive regulator of JA production. By contrast, plasma membrane displacement versus the wall upon hyperosmotic shock would remove THE1-mediated repression of ABA production.

In our model, THE1 acts as positive or negative regulator dependent on changes in the cell wall–plasma membrane continuum (25). Such context-dependent behavior has been described for FER and explained by FER acting as scaffold interacting with a large number of partners, bringing about specific activities (25). However, manipulating FER activity has profound phenotypic effects, while loss of THE1 activity has only limited consequences. More importantly, FER acts as negative regulator for salt stress–induced ABA and ISX-induced JA, SA, and lignin production, while THE1 is a positive regulator for ISX-induced JA, SA, and lignin production (13, 47). This suggests that some form of redundancy compensates for loss of THE1 and that THE1 has more specialized and different (opposing) functions than FER, even if both FER and THE1 contribute to stress-induced, cell wall–dependent processes. Redundancy could be

mediated by other molecular components involved in mechano-perception or coordination between the cell wall and cellular components (3, 4, 24, 48).

Reduced JA induction in *rlp12* seedlings after ISX treatment and ISX-induced, osmosensitive *RLP12* expression in the same region of the root-like *THE1* indicate that *RLP12* is required for CWI maintenance. *RLP12* has been implicated previously in osmosensitive and biotic, stress-related processes (40). The reduced JA production in *rlp12* seedlings is similar to reductions observed for *LRR-RK MALE DISCOVERER 1-INTERACTING RECEPTOR LIKE KINASE 2/LEUCINE-RICH REPEAT KINASE FAMILY PROTEIN INDUCED BY SALT STRESS* (*MIK2/LRR-KISS*) mutants (49). In contrast, other mutations in leucine-rich repeat kinases required for pattern-triggered immunity enhance ISX-induced JA production (13, 49). A possible explanation is that RLP12 has a specific function in CWI maintenance, with effects on biotic stress response being only secondary consequences. The limited mutant phenotypes observed in *the1* and *rlp12* adult plants suggest that both genes are either primarily required at the seedling stage or redundancy may exist.

To summarize, here we have used Brillouin microscopy to investigate processes modifying cell wall stiffness in plants in vivo. The results illustrate the application potential for Brillouin microscopy and how it can complement other recently developed methods (6, 50–52). Based on the data generated, we suggest that THE1 is a key regulatory element enabling a plant cell to differentially activate phytohormone production upon exposure to either CWD or hyperosmotic, stress-induced membrane displacement. The ability to differentially activate phytohormones in a tightly controlled manner is, in turn, a key prerequisite for successful plant adaptation to a changing environment, where extreme biotic and abiotic stress situations become the norm not the exception (9, 22).

Materials and Methods

Plant Material. *A. thaliana* and *P. sativum* genotypes used in this study were obtained from the laboratories previously publishing them or ordered from the Nottingham *Arabidopsis* Stock Centre (arabidopsis.info/). Detailed information is listed in *SI Appendix*, Table S1.

Plant Growth Conditions. *Arabidopsis* seedlings were grown in sterile conditions in liquid culture or on plates, as described in ref. 11, with minor modifications. A total of 30 mg seeds were sterilized by sequential incubation with 70% ethanol and 50% bleach on a rotating mixer for 10 min each and washed three times with sterile water. Seeds were then transferred into 250-mL Erlenmeyer flasks containing 125 mL half-strength Murashige and Skoog growth medium (2.1 g · L^{-1} Murashige and Skoog Basal Medium, 0.5 g · L^{-1} sodium 2-(4-morpholinyl)ethanesulfonate salt, and 1% sucrose at pH 5.7). Seedlings were grown in long-day conditions (16 h light, 22 °C/8 h dark, and 18 °C) at 150 µmol · m^{-2} · s^{-1} photon flux density on an IKA KS501 flask shaker at a constant speed of 130 rotations per minute.

For histochemical GUS staining and microscopy imaging, *Arabidopsis* seeds were sterilized, and three to five individual seeds were placed in a well of a clear 6-well tissue culture plate and grown in the described liquid media and growth conditions.

For experiments with protoplasts and turgor loss point measurements, *Arabidopsis* seeds were sown directly in 10-cm pots containing a 90:10 (v · v^{-1}) mix of peat moss:fine grade vermiculite. Pots were sat in trays of water and covered in clear plastic wrap for 5 d until seeds had germinated, after which the plastic wrap was removed, and plants were thinned to one per pot. Pots were watered by immersion every 3 d and received a weekly watering of liquid fertilizer (Miracle-Gro, Scotts Miracle-Gro). Short-day growth conditions were maintained, under a 10-h photoperiod, provided by LED lighting, resulting in a photosynthetically active radiation (PAR) of 50 µmol · m^{-2} · s^{-1} at pot height. Temperature was maintained at 23 °C. Experiments were conducted on the newest fully expanded leaves of plants that were at least 5 wk of age.

Seeds of *P. sativum* genotype Argenteum were grown in 14-cm pots containing a 1:1 (v · v^{-1}) mix of vermiculite and dolerite chips topped with 4 cm fine, pine bark–potting mix. Plants were grown in a greenhouse under a 16-h photoperiod; supplemented and extended by sodium vapor lamps, which provided a minimum PAR of 300 µmol · m^{-2} · s^{-1} at pot height; and a 23/16 °C day/night temperature cycle.

Protoplasts were prepared from ~20 newest, fully expanded leaves of *Arabidopsis* genotypes and *P. sativum*, as described in ref. 53, using cellulase and pectinase enzymes; isolated mesophyll cells were prepared from a similar amount of material, as described in ref. 44, using only pectinase enzymes to ensure walls were retained. Once isolated, protoplasts or mesophyll cells were suspended in an aqueous solution of PEG (MW 3000) prepared to a water potential of −0.3 or −1 MPa, according to ref. 54, for 1 h. Leaves of *Arabidopsis* or *P. sativum* (with epidermis removed) were also excised under water and sliced into 2-mm strips, then suspended in aqueous PEG solutions set at either −0.3 or −1 MPa, vacuum infiltrated, and incubated for 1 h. After exposure to PEG solutions, leaf samples and solutions containing protoplasts or isolated mesophyll cells were immersed in cold −20 °C 80% methanol in water (v · v^{-1}) with added butylated hydroxytoluene (250 mg · L^{-1}) for ABA analysis. Leaf samples were removed from PEG solutions and dried briskly on paper towel before being covered in methanol solution. At least three times, the volume of methanol was added to protoplast or isolated mesophyll cell solutions. All experiments were repeated four times.

Plants for gas exchange measurements were grown in 2:1 (v · v^{-1}) peat:vermiculite mixture, as previously described (55). Plants were grown in growth chambers (AR-66LX, Percival Scientific, and Snijders Scientific) with 12-h photoperiod, 23/18 °C day/night temperature, 150 µmol · m^{-2} · s^{-1} light, and 70% relative humidity. Plants were 24 to 28 d old during gas exchange experiments.

CWD was generated in *Arabidopsis* seedlings using the cellulose biosynthesis inhibitor ISX at a concentration of 600 nM in half-strength Murashige and Skoog growth medium. To generate hyperosmotic stress, the growth medium was supplemented with 300 mM sorbitol. Additional treatments include the combination of ISX and sorbitol (600 nM ISX + 300 mM sorbitol) and treatment with dimethylsulfoxide (DMSO) as mock control (solvent for ISX). Standard treatment duration was 6 h, unless specified differently.

Root Growth Assays. Seedlings were grown for 6 d on plates containing growth medium with the same composition as the liquid medium but containing, in addition, 0.8% Agarose (Sigma). Seedlings were transferred from regular plates to plates either 10 µM ABA or no ABA (GM). Positions of root tips were marked after transfer, and then, roots were allowed to grow for 24 h. After 24 h, images were taken using a Zeis Axio Zoom.V16 equipped with a PlanNeoFluar Z 1×/0.25 FWD 56 mm objective lens, a 25×/10foc eyepiece, and a Zeiss Axiocam506 color. Root lengths were determined using the freehand drawing tool in Fiji Version 2.1.0. Three independent experiments were performed, and for each treatment/genotype combination, >15 seedling roots were measured per experiment. For calculation of relative root length, the following formula was applied:

$$\text{Relative root size} = \frac{\text{Root size (ABA treatment)}}{\text{Average root size in GM}}.$$

Microscopy.

Brillouin microscopy. Brillouin spectra were acquired using two different interferometers: Automatized time course data were recorded using a virtually imaged phased array (VIPA)–based system that offers typically 2-s acquisition times, and complementary measurements were obtained using a Tandem Fabry Perot (TFP) interferometer. The spectrometers are both coupled with an inverted life science microscope (Eclipse Ti-U, Nikon) equipped with a micropositioning stage. The collimated, linearly polarized laser light (532-nm single-mode laser, Spectra-Physics Excelsior-532), spectral linewidth < 0.01 PM) is focused onto the sample using a 20× objective lens with a numerical aperture (NA) of 0.35. The focal plans were adjusted on Col-0 roots, near the equatorial plan of the roots. The typical power used at the focus was 8 mW. The backscattered light is collected by the same objective lens and is collected outside the microscope using a telescope.

The TFP interferometer (JRS Scientific Instruments) offers a 15-GHz free spectral range (FSR) sampled with a 30-MHz resolution. It is equipped with two sets of mirrors with a 95% reflectivity and an avalanche photodiode (Count R Blue, Laser Components) with a dark count lower than 10 counts/s (typically 2 counts/s) and a quantum efficiency of 65% at this wavelength. The magnification of the telescope that collects the backscattered light is calculated to be in accordance with the size of the 300-µm entrance pinhole of the spectrometer. Each spectrum is acquired by averaging over ~150 counts to obtain a 13-dB noise level, typically (56).

The VIPA spectrometer (Light Machinery, Hyperfine HF-8999-532) is based on a 3.37-mm thick VIPA etalon (30 GHz, 500 to 600 nm) and is equipped with two double-passed, air-spaced etalons to increase the contrast to about 120 dB. The fiber is directly connected to the built-in FC/PC connector of the VIPA spectrometer. The FSR of the VIPA used in our work is 30 GHz, corresponding to a sampling interval of 0.11 GHz. Typical acquisitions times were 5 s per point (31).

To determine the part of the *Arabidopsis* root responsive to CWD, 6-d-old seedlings (Col-0 and *ixr1-1* as control), grown as described in *Plant Growth Conditions* were treated for 6 h with 600 nM ISX. Five regions on the roots were visually identified in each genotype for both ISX- and mock (DMSO)-treated seedlings. The regions correspond to different developmental stages (differentiation zone, elongation zone, transition zone, basal meristem, and apical meristem; *SI Appendix*, Fig. S2A). Brillouin spectroscopy measurements were acquired logitudinal in each zone, starting 250 μm away from the root tip (15 μm between points) for three different tissue layers identified visually: stele, endodermis, and epidermis (*SI Appendix*, Fig. S2B). The results were analyzed, and the end of the basal meristem was chosen as the target region for the next experiments (*SI Appendix*, Fig. S2B). To determine the effects of CWD and turgor pressure on cell wall stiffness, different treatments were performed for each genotype using the same plant material as described previously: 1) mock treatment, 2) CWD (600 nM ISX); 3) hyperosmotic pressure (300 mM sorbitol); and 4) combined treatment (600 nM ISX + 300 mM sorbitol). Samples (at least three per replicate, three replicates) were collected at times 0 and 6, after the start of treatments for each genotype. The central point in the X-axis at the end of the basal meristem (at around 450 μm from the root tip) was visually identified (*SI Appendix*, Fig. S2C) and a point 180 μm to the left from the center of the root was selected as the starting point for collecting measurements after being sure that this point was in the water. Brillouin spectroscopy measurements were then acquired in each zone (15 μm between points).

Initial data analysis was performed in Matlab (MathWorks) using custom written scripts. Before the analysis, we verified that the average noise (measured in the spectral regions without any Brillouin peaks) is zero. Assuming a moderate attenuation in our systems, we fit the spectra with a Lorentzian function to determine the Brillouin frequency shift. This procedure allows us to reach a 6-MHz accuracy at a 10-dB noise level. Further processing included the calculation of Brillouin Elastic Contrast, as defined in ref. 6:

$$\bar{\nu}_B = \frac{\nu_B}{\nu_B^w} - 1,$$

where ν_B and ν_B^w are the frequency shifts measured in the sample and in distilled water, respectively.

$\bar{\nu}_B$ is a dimensionless parameter that normalizes the obtained Brillouin frequency shifts to those obtained for distilled water using the same setup as for the sample. Regression curves were fitted for each graph using smooth conditional medias (from ggplot2 R package) calculated using local polynomial regression fitting (LOESS) method.

Confocal microscopy. Fluorescence confocal laser-scanning microscopy was performed using a Leica TCS SP8 (Leica Microsystems) for reporter lines *pJAZ10::YFP* and *pRAB18::GFP-GUS* and LSM 800 (Carl Zeiss) for reporter line *pTHE::YFP*. Seedlings were stained in the respective treatment media supplemented with 0.1% Calcofluor White Stain solution for 30 min and rinsed for 5 to 10 times in pure treatment media before imaging. Seedlings were mounted in treatment media. Image acquisition was done with HC PL APO CS 10×/0.40 NA dry and HC PL APO CS2 20×/0.75 NA dry objectives in Leica TCS SP8 (Leica Microsystems). Calcofluor White was excited at a 405-nm laser, and emission was detected between 425 to 475 nm. YFP/GFP was excited at 514 nm, and emission was detected between 519 to 553 nm in Leica TCS SP8 (Leica Microsystems). The acquisition for LSM 800 (Carl Zeiss) was done with Plan-Neofluar 10×/0.3 NA dry objective in LSM 800 (Carl Zeiss), and samples were imaged using the excitation laser line 405 nm, and emission was detected at 400 to 470 nm for Calcofluor White fluorescence detection, and the excitation laser line 488 nm and emission spectrum was detected at 507 to 700 nm for YFP. Images obtained from Leica TCS SP8 (Leica Microsystems) were processed in Fiji (ImageJ), and images obtained from LSM 800 (Carl Zeiss) were processed as single plane maximum intensity projections of three optical sections in Zen Blue 3.3 software (Carl Zeiss).

Histochemical GUS Staining. The 7-d-old seedlings were mock, ISX, sorbitol, or an ISX/sorbitol treated for 6 h and submerged into GUS staining solution [50 mM phosphate buffer (pH = 7), 2 mM ferricyanide K_3Fe(CN)_6, 2 mM ferrocyanide {K_4Fe(CN)_6*3H_2O}, 2 mM 5-Bromo-4-chloro-3-indolyl β-D-glucopyranoside (X-Glc), and 0.2% Triton X-100] immediately after. The samples were incubated for 60 min at 37 °C in darkness and transferred to 70% ethanol for 2 d (at RT) prior to imaging. Seedlings were imaged with a Zeiss Axio Zoom.V16 equipped with a PlanNeoFluar Z 1×/0.25 FWD 56-mm objective lens, a 25×/10foc eyepiece, and a Zeiss Axiocam506 color. For image acquisition, intensity of the Zeiss CL 9000 LED light source was set to 21%. Other settings used were a fully opened aperture, motorized zoom factor of 5.1× (resulting in a final root magnification of 128×), and an exposure time of 150 ms.

Phytohormone Measurements. JA and ABA were analyzed as described (57), with minor modifications. *Arabidopsis* seedlings were flash frozen in liquid nitrogen and freeze dried for 24 h. A total of 6- to 7-mg aliquots of freeze-dried seedlings were ground with 5-mm stainless steel beads in a Qiagen Tissue Lyser II for 2 min at 25 Hz. Shaking was repeated after the addition of 400 μL extraction buffer (10% methanol, 1% acetic acid) with internal deuterated standards (50 ng · mL^{-1} Jasmonic-d$_5$ acid, 50 ng mL^{-1} Salicylic-D$_4$ acid, and 10 ng mL^{-1} Abscisic-D$_6$ acid; CDN Isotopes) before samples were incubated on ice for 30 min and centrifuged for 10 min at 16,000 × g and 4 °C. Supernatants were transferred into fresh tubes and centrifuged three times to remove all debris prior to liquid chromatography with tandem mass spectrometry (LC-MS/MS) analysis. An extraction control not containing plant material was treated equally to the plant samples.

Chromatographic separation was carried out on a Waters ACQUITY I Class UPLC system, equipped with a Waters Cortecs C18 column (2.7 mm, 2.1 × 100 mm). Water was used as mobile phase A, and acetonitrile was used as mobile phase B, both containing 0.1% formic acid. The linear mobile phase gradient was adapted to a total run time of 7 min: 0 to 4 min 20 to 95% B, 4 to 5 min 95% B, 5 to 7 min 95 to 20% B; and flow rate 0.4 mL/min. The column temperature was maintained at 35 °C; the injection volume was 5 μL.

For hormone detection and quantification, a Waters Xevo TQ-XS triple quadrupole mass spectrometer was employed. The mass spectrometer was equipped with an electrospray ionization (ESI) source operated in negative mode, and MS conditions were set as follows: capillary voltage −1.8 kV; cone voltage 25 V; source offset voltage 30 V; source temperature 150 °C; desolvation temperature 500 °C; cone gas flow 150 L · h^{-1}; desolvation gas flow 1,000 L · h^{-1}; collision gas flow 0.15 mL · min^{-1}; and nebulizer gas flow 6 Bar. The spectra were acquired in multiple reactions monitoring mode and following precursor–product ion transitions were used for quantification: JA 209.10 > 58.98, D$_5$-JA 214.10 > 62.00, SA 136.97> 93.20, D$_4$-SA 140.97 > 97.20, ABA 263.00 > 153.00, and D$_6$-ABA 269.00 > 159.00.

Individual stock solutions of phytohormones were prepared in methanol. A series of standard mixes in the range of 0.2 to 1,000 ng/mL, prepared in extraction solvent containing deuterated internal standards, and were used to build up calibration curves.

ABA levels in *A. thaliana* and *P. sativum* protoplasts and leaves were quantified physicochemically with an added internal standard, according to the method previously described (58), using an Agilent 6400 Series Triple Quadrupole liquid chromatograph tandem mass spectrometer. To remove excess PEG from samples, the sample in 200 μL 2% acetic acid in water (v · v^{-1}) was purified by partitioning twice with 100 μL diethyl ether and with the organic phase containing the ABA dried to completeness at 40 °C, after the sample was resuspended in 200 μl 2% acetic acid in water (v · v^{-1}). ABA samples in *P. sativum* were prepared similarly to those of *Arabidopsis* but were quantified physicochemically with an added internal standard according using a ultra performance LC-MS/MS (UPLC-MS/MS), as previously described in (59).

Generation of Transgenic Lines. Genomic DNA (gDNA) was extracted from 7-d-old *Arabidopsis* Col-0 seedlings with E.Z.N.A Plant DNA kit (Omega). The full-length *RLP12* promoter (*pRLP12*) was amplified using gDNA as template with primer pairs containing AttB1/2 recombination sites (*SI Appendix*, Table S2). *pRLP12* was inserted through Gateway Recombination Cloning Technology (Life Technologies) in the binary pFAST-G02 (containing GFP-GUS fusion) vector (60) used as destination. Upon *Agrobacterium*-mediated transformation, we selected, by using Zeiss Axio Zoom V16 equipped with fluorescence filters for GFP, seven independents transgenic stable T1 plants (in Col-0 background). Experiments were carried on two homozygous T3 lines.

Transcriptomics. Total RNA was extracted using a Spectrum Plant Total RNA Kit (Sigma-Aldrich). RNA integrity was assessed using an Agilent RNA6000 Pico Kit. Sequencing samples were prepared and analyzed as described previously (14). The intersection of the DE genes between the treatments was visualized using a Venn diagram produced with R package BioVenn (61).

qRT-PCR–Based Gene Expression Analysis. Total RNA was isolated using a Spectrum Plant Total RNA Kit (Sigma-Aldrich). A total of 2 mg total RNA were treated with RQ1 RNase-Free DNase (Promega) and processed with the ImProm-II Reverse Transcription System (Promega) for complementary DNA-synthesis. qRT-PCR was performed using a LightCycler 480 SYBR Green I Master (Roche) and primers (*SI Appendix*, Table S2) diluted according to manufacturer specifications. *ACT2* is used as reference in all experiments (13). The expression levels of each gene were determined using the Pfaffl method (62). All experiments were repeated at least three times.

Stomatal Conductance Measurements. Stomatal conductance of plants was measured using a rapid response gas exchange measurement device consisting of eight thermostated, flow-through, whole-rosette cuvettes. Plants were inserted into the cuvettes in the morning, and when their stomatal conductance

Bacete et al.
THESEUS1 modulates cell wall stiffness and abscisic acid production
in *Arabidopsis thaliana*

had stabilized, darkness was applied for 2 h. Subsequently, light was applied to register light-induced increase of stomatal conductance within next 2 h. To study ABA-induced stomatal closure, plants were sprayed with 5 μM ABA solution with 0.012% Silwet L-77 (Duchefa) and 0.05% ethanol, as described previously (37). ABA-induced changes in stomatal conductance were examined at gs18 and gs0, in which gs0 is the pretreatment stomatal conductance and gs18 is the value of stomatal conductance 18 min after ABA spraying.

Pressure–Volume Curve Analysis. Pressure–volume curves were used to determine leaf turgor loss point in five leaves from each *Arabidopsis* genotype according to the methods of ref. 63. Briefly, the petioles of leaves were excised under water and rehydrated overnight in a sealed bag. Leaves were imaged to determine leaf area, and then, concurrent and periodic measurements of leaf mass (± 0.0001 g) and water potential were conducted using a Scholander pressure chamber with microscope to determine the balance pressure until at least three measurements had been collected in each leaf past turgor loss point. Leaves were then dried at 70 °C and weighed to determine dry mass.

Cell Wall Analysis. *Arabidopsis* seedlings or leaves were lyophilized and ball milled in a Retsch mixer mill. All samples were extracted three times with 70% ethanol at 70 °C, washed with acetone, and dried in a vacuum concentrator. The alcohol-insoluble residue was weighed out in 2-mL screw caps tubes and used for extraction of neutral cell wall sugars, uronic acids, and cellulose, as described (64). High-performance anion exchange chromatography with pulsed amperometric detection was performed on a biocompatible Knauer Azura HPLC system, equipped with an Antec Decade Elite SenCell detector. Monosaccharides were separated on a Thermo Fisher Scientific Dionex Carbo-Pac PA20 column with a solvent gradient of 1) water, 2) 10 mM NaOH, and 3) 700 mM NaOH at 0.4 mL · min^{-1} flow rate and 40 °C column/detector temperature. 0 to 25 min: 20% B, 25 to 28 min: 20 to 0% B, 0 to 70% C, 28 to 33 min: 70% C, 33 to 35 min: 70 to 100% C, 35 to 38 min: 100% C, 38 to 42 min: 0 to 20% B, 100 to 0% C, and 42 to 60 min: 20% B.

Statistical Analysis. Statistical significance of data under normal distribution was tested using either Student's *t* test or one-way ANOVA followed by post hoc analysis with Tukey's honest significant difference test. Statistical details of experiments are specified in the figure legends. In the case of data not following normal distribution [as indicated by Shapiro–Wilk test at $\alpha = 0.05$ (65)], a nonparametric test (Wilcoxon rank sum test, multiple comparisons corrected with continuous correction) was performed. Statistically significant differences are indicated by *$P < 0.05$, **$P < 0.01$, and ***$P < 0.001$ paired comparisons, and different letters are used for multiple comparisons at $\alpha = 0.05$. Statistical analyses were performed in R (66) using the packages ggplot2 (67), dplyr (68), multcomp (69), and lsmeans (70).

Data Availability. Transcripmoics data have been deposited in Gene Expression Omnibus (GSE109613). All other study data are included in the article and/or supporting information.

1. W. J. Barnes, C. T. Anderson, Release, recycle, rebuild: Cell-wall remodeling, autodegradation, and sugar salvage for new wall biosynthesis during plant development. *Mol. Plant* **11**, 31–46 (2018).
2. L. Bacete, H. Mélida, E. Miedes, A. Molina, Plant cell wall-mediated immunity: Cell wall changes trigger disease resistance responses. *Plant J.* **93**, 614–636 (2018).
3. O. Hamant, E. S. Haswell, Life behind the wall: Sensing mechanical cues in plants. *BMC Biol.* **15**, 59 (2017).
4. A. Sampathkumar, Mechanical feedback-loop regulation of morphogenesis in plants. *Development* **147**, dev177964 (2020).
5. N. Hoffmann, S. King, A. L. Samuels, H. E. McFarlane, Subcellular coordination of plant cell wall synthesis. *Dev. Cell* **56**, 933–948 (2021).
6. G. Antonacci et al., Recent progress and current opinions in Brillouin microscopy for life science applications. *Biophys. Rev.* **12**, 615–624 (2020).
7. A. J. Bidhendi, A. Geitmann, Methods to quantify primary plant cell wall mechanics. *J. Exp. Bot.* **70**, 3615–3648 (2019).
8. S. V. Adichtchev et al., Brillouin spectroscopy of biorelevant fluids in relation to viscosity and solute concentration. *Phys. Rev. E* **99**, 062410 (2019).
9. L. Vaahtera, J. Schulz, T. Hamann, Cell wall integrity maintenance during plant development and interaction with the environment. *Nat. Plants* **5**, 924–932 (2019).
10. T. Hamann, M. Bennett, J. Mansfield, C. Somerville, Identification of cell-wall stress as a hexose-dependent and osmosensitive regulator of plant responses. *Plant J.* **57**, 1015–1026 (2009).
11. L. Denness et al., Cell wall damage-induced lignin biosynthesis is regulated by a reactive oxygen species- and jasmonic acid-dependent process in *Arabidopsis. Plant Physiol.* **156**, 1364–1374 (2011). Correction in: *Plant Physiol.* **168**, 1181–1182 (2015).
12. A. Wormit et al., Osmosensitive changes of carbohydrate metabolism in response to cellulose biosynthesis inhibition. *Plant Physiol.* **159**, 105–117 (2012).
13. T. Engelsdorf et al., The plant cell wall integrity maintenance and immune signaling systems cooperate to control stress responses in *Arabidopsis thaliana. Sci. Signal.* **11**, eaao3070 (2018).
14. N. Gigli-Bisceglia et al., Cell wall integrity modulates *Arabidopsis thaliana* cell cycle gene expression in a cytokinin- and nitrate reductase-dependent manner. *Development* **145**, dev166678 (2018).
15. L. Bacete, T. Hamann, The role of mechano-perception in plant cell wall integrity maintenance. *Plants (Basel)* **9**, 574 (2020).
16. E. W. Chehab, C. Yao, Z. Henderson, S. Kim, J. Braam, *Arabidopsis* touch-induced morphogenesis is jasmonate mediated and protects against pests. *Curr. Biol.* **22**, 701–706 (2012).
17. C. M. Franck, J. Westermann, A. Boisson-Dernier, Plant malectin-like receptor kinases: From cell wall integrity to immunity and beyond. *Annu. Rev. Plant Biol.* **69**, 301–328 (2018).
18. K. Hématy et al., A receptor-like kinase mediates the response of *Arabidopsis* cells to the inhibition of cellulose synthesis. *Curr. Biol.* **17**, 922–931 (2007).
19. S. Qu, X. Zhang, Y. Song, J. Lin, X. Shan, THESEUS1 positively modulates plant defense responses against *Botrytis cinerea* through GUANINE EXCHANGE FACTOR4 signaling. *J. Integr. Plant Biol.* **59**, 797–804 (2017).
20. M. Gonneau et al., Receptor kinase THESEUS1 is a rapid alkalinization factor 34 receptor in *Arabidopsis. Curr. Biol.* **28**, 2452–2458.e4 (2018).
21. J. Chen et al., FERONIA interacts with ABI2-type phosphatases to facilitate signaling cross-talk between abscisic acid and RALF peptide in *Arabidopsis. Proc. Natl. Acad. Sci. U.S.A.* **113**, E5519–E5527 (2016).
22. A. Gupta, A. Rico-Medina, A. I. Caño-Delgado, The physiology of plant responses to drought. *Science* **368**, 266–269 (2020).
23. W. Feng et al., The FERONIA receptor kinase maintains cell-wall integrity during salt stress through Ca 2+ signaling. *Curr. Biol.* **28**, 666–675.e5 (2018).
24. K. Dünser et al., Extracellular matrix sensing by FERONIA and leucine-rich repeat extensins controls vacuolar expansion during cellular elongation in *Arabidopsis thaliana. EMBO J.* **38**, e100353 (2019).
25. M. Stegmann et al., The receptor kinase FER is a RALF-regulated scaffold controlling plant immune signaling. *Science* **355**, 287–289 (2017).
26. F. Takahashi, T. Kuromori, K. Urano, K. Yamaguchi-Shinozaki, K. Shinozaki, Drought stress responses and resistance in plants: From cellular responses to long-distance intercellular communication. *Front. Plant Sci.* **11**, 556972 (2020). Correction in: *Front Plant Sci.* **12**, 703149 (2021).
27. T. Dong, Y. Park, I. Hwang, Abscisic acid: Biosynthesis, inactivation, homoeostasis and signalling. *Essays Biochem.* **58**, 29–48 (2015).
28. S. A. M. McAdam, T. J. Brodribb, Mesophyll cells are the main site of abscisic acid biosynthesis in water-stressed leaves. *Plant Physiol.* **177**, 911–917 (2018).
29. R. Hedrich, Ion channels in plants. *Physiol. Rev.* **92**, 1777–1811 (2012).
30. K. Komatsu, D. Takezawa, Y. Sakata, Decoding ABA and osmostress signalling in plants from an evolutionary point of view. *Plant Cell Environ.* **43**, 2894–2911 (2020).
31. G. Yan, A. Bazir, J. Margueritat, T. Dehoux, Evaluation of commercial virtually imaged phase array and Fabry-Pérot based Brillouin spectrometers for applications to biology. *Biomed. Opt. Express* **11**, 6933–6944 (2020).
32. D. Merz et al., T-DNA alleles of the receptor kinase THESEUS1 with opposing effects on cell wall integrity signaling. *J. Exp. Bot.* **68**, 4583–4593 (2017).
33. Y.-N. Deng et al., Structure and activity of SLAC1 channels for stomatal signaling in leaves. *Proc. Natl. Acad. Sci. U.S.A.* **118**, e2015151118 (2021).
34. C. Ellis, J. G. Turner, The *Arabidopsis* mutant cev1 has constitutively active jasmonate and ethylene signal pathways and enhanced resistance to pathogens. *Plant Cell* **13**, 1025–1033 (2001).
35. S. A. M. McAdam, T. J. Brodribb, Linking turgor with ABA biosynthesis: Implications for stomatal responses to vapor pressure deficit across land plants. *Plant Physiol.* **171**, 2008–2016 (2016).
36. P. Marhavý et al., Single-cell damage elicits regional, nematode-restricting ethylene responses in roots. *EMBO J.* **38**, e100972 (2019).
37. E. Merilo et al., Stomatal VPD response: There is more to the story than ABA. *Plant Physiol.* **176**, 851–864 (2018).
38. C. de Ollas, I. C. Dodd, Physiological impacts of ABA-JA interactions under water-limitation. *Plant Mol. Biol.* **91**, 641–650 (2016).
39. J. Braam, R. W. Davis, Rain-, wind-, and touch-induced expression of calmodulin and calmodulin-related genes in *Arabidopsis. Cell* **60**, 357–364 (1990).
40. G. Wang et al., Functional analyses of the CLAVATA2-like proteins and their domains that contribute to CLAVATA2 specificity. *Plant Physiol.* **152**, 320–331 (2010).

Bacete et al.
THESEUS1 modulates cell wall stiffness and abscisic acid production in *Arabidopsis thaliana*

PNAS | 9 of 10
https://doi.org/10.1073/pnas.2119258119

41. M. Gonzalez-Guzman *et al.*, *Arabidopsis* PYR/PYL/RCAR receptors play a major role in quantitative regulation of stomatal aperture and transcriptional response to abscisic acid. *Plant Cell* **24**, 2483–2496 (2012).

42. S. H. Schwartz, K. M. Léon-Kloosterziel, M. Koornneef, J. A. Zeevaart, Biochemical characterization of the aba2 and aba3 mutants in *Arabidopsis thaliana*. *Plant Physiol.* **114**, 161–166 (1997).

43. S.-D. Zhu *et al.*, Leaf turgor loss point is correlated with drought tolerance and leaf carbon economics traits. *Tree Physiol.* **38**, 658–663 (2018).

44. B. Colman, B. T. Mawson, The role of plasmolysis in the isolation of photosynthetically active leaf mesophyll cells. *Z. Pflanzenphysiol.* **86**, 331–338 (1978).

45. B. T. Mawson, B. Colman, W. R. Cummins, Abscisic acid and photosynthesis in isolated leaf mesophyll cell. *Plant Physiol.* **67**, 233–236 (1981).

46. M. Pierce, K. Raschke, Correlation between loss of turgor and accumulation of abscisic acid in detached leaves. *Planta* **148**, 174–182 (1980).

47. S. Zhu, Q. Fu, F. Xu, H. Zheng, F. Yu, New paradigms in cell adaptation: Decades of discoveries on the *Cr*RLK1L receptor kinase signalling network. *New Phytol.* **232**, 1168–1183 (2021).

48. A. Malivert *et al.*, FERONIA and microtubules independently contribute to mechanical integrity in the *Arabidopsis* shoot. *PLoS Biol.* **19**, e3001454 (2021).

49. D. Van der Does *et al.*, The *Arabidopsis* leucine-rich repeat receptor kinase MIK2/LRR-KISS connects cell wall integrity sensing, root growth and response to abiotic and biotic stresses. *PLoS Genet.* **13**, e1006832 (2017).

50. L. Michels *et al.*, Complete microviscosity maps of living plant cells and tissues with a toolbox of targeting mechanoprobes. *Proc. Natl. Acad. Sci. U.S.A.* **117**, 18110–18118 (2020).

51. S. Robinson *et al.*, An automated confocal micro-extensometer enables in vivo quantification of mechanical properties with cellular resolution. *Plant Cell* **29**, 2959–2973 (2017).

52. K. Elsayad *et al.*, Mapping the subcellular mechanical properties of live cells in tissues with fluorescence emission-Brillouin imaging. *Sci. Signal.* **9**, rs5 (2016).

53. S.-D. Yoo, Y.-H. Cho, J. Sheen, *Arabidopsis* mesophyll protoplasts: A versatile cell system for transient gene expression analysis. *Nat. Protoc.* **2**, 1565–1572 (2007).

54. A. A. Steuter, A. Mozafar, J. R. Goodin, Water potential of aqueous polyethylene glycol. *Plant Physiol.* **67**, 64–67 (1981).

55. T. Kollist *et al.*, A novel device detects a rapid ozone-induced transient stomatal closure in intact *Arabidopsis* and its absence in abi2 mutant. *Physiol. Plant.* **129**, 796–803 (2007).

56. J. Margueritat *et al.*, High-frequency mechanical properties of tumors measured by Brillouin light scattering. *Phys. Rev. Lett.* **122**, 018101 (2019).

57. S. Forcat, M. H. Bennett, J. W. Mansfield, M. R. Grant, A rapid and robust method for simultaneously measuring changes in the phytohormones ABA, JA and SA in plants following biotic and abiotic stress. *Plant Methods* **4**, 16 (2008).

58. A. A. Cardoso, J. M. Randall, S. A. M. McAdam, Hydraulics regulate stomatal responses to changes in leaf water status in the fern *Athyrium filix-femina. Plant Physiol.* **179**, 533–543 (2019).

59. S. McAdam, Physicochemical quantification of abscisic acid levels in plant tissues with an added internal standard by ultra-performance liquid chromatography. *Bio Protoc.* **5**, e1599 (2015).

60. T. L. Shimada, T. Shimada, I. Hara-Nishimura, A rapid and non-destructive screenable marker, FAST, for identifying transformed seeds of *Arabidopsis thaliana. Plant J.* **61**, 519–528 (2010). Correction in: *Plant J.* **63**, 352 (2010).

61. T. Hulsen, J. de Vlieg, W. Alkema, BioVenn - A web application for the comparison and visualization of biological lists using area-proportional Venn diagrams. *BMC Genomics* **9**, 488 (2008).

62. M. W. Pfaffl, A new mathematical model for relative quantification in real-time RT-PCR. *Nucleic Acids Res.* **29**, e45 (2001).

63. M. Tyree, H. Hammel, The measurement of the turgor pressure and the water relations of plants by the pressure-bomb technique. *J. Exp. Bot.* **23**, 267–282 (1972).

64. T. Yeats, T. Vellosillo, N. Sorek, A. Ibáñez, S. Bauer, Rapid determination of cellulose, neutral sugars, and uronic acids from plant cell walls by one-step two-step hydrolysis and HPAEC-PAD. *Bio Protoc.* **6**, e1978 (2016).

65. S. S. Shapiro, M. B. Wilk, An analysis of variance test for normality (complete samples). *Biometrika* **52**, 591–611 (1965).

66. R Core Team, R: A language and environment for statistical computing (R Foundation for Statistical Computing, 2020).

67. H. Wickham, *ggplot2: Elegant Graphics for Data Analysis* (Springer, New York, NY, 2016).

68. H. Wickham, R. François, L. Henry, K. Müller, dplyr: A grammar of data manipulation. R package version 1.0.7. https://CRAN.R-project.org/package=dplyr. Accessed 16 December 2021.

69. T. Hothorn, F. Bretz, P. Westfall, Simultaneous inference in general parametric models. *Biom. J.* **50**, 346–363 (2008).

70. R. V. Lenth, Least-squares means: The R package lsmeans. *J. Stat. Softw.* **69**, 1–33 (2016).

10 of 10 | **PNAS**
https://doi.org/10.1073/pnas.2119258119

Bacete et al.
THESEUS1 modulates cell wall stiffness and abscisic acid production
in *Arabidopsis thaliana*